Assessment of VIV fatigue of subsea template jumper by using a time domain model

Linda Sieber
OffNoise-HSD-Systems, Hannover, Germany

Svein Sævik
Department of Marine Technology, Norwegian University of Science and Technology, Trondheim, Norway

Jonas Ringsberg
Department of Mechanics and Maritime Sciences, Chalmers University of Technology, Gothenburg, Sweden

Zhenhui Liu
Department of Engineering, Aker Solutions AS, Trondheim, Norway

ABSTRACT: This paper addresses the application of a time domain model for Vortex-Induced Vibration (VIV) to assess the fatigue damage of subsea jumpers. The time domain model, capable of accounting for structural non-linearity and time-varying flow, was applied on a typical 'M'-shaped jumper model. Obtained results were compared against VIV motion data from experiments in the literature. Fatigue estimates were also compared to the DNVGL response model approach. Two models were investigated, with and without elbow elements in the bends. The reduced stiffness of the model including elbow elements improved the results of modal analysis and caused a shift in the mode shape order. VIV motion results were in good correlation with model test data. With several exceptions, the fatigue damage calculated using the DNVGL response model procedure was higher than obtained from the time domain model, as no mode competition is applied on non-straight pipes. For several load cases torsion stress was the largest stress component.

1 INTRODUCTION

In the offshore industry, rigid jumpers are often placed close to the seabed in the environment of low-velocity currents. These currents can induce vortex induced vibration (VIV) of the structures as a result of oscillating forces from the fluid. VIV can lead to a large number of load cycles, which significantly decreases the life of the structures. For environmental and economic reasons, the prediction of VIV is therefore of high importance in fatigue life assessment.

Semi-empirical models in frequency domain, such as VIVANA (Larsen et al., 2017), Shear7 (Vandiver and Li, 2005), and VIVA (Triantafyllou et al., 1999) have been developed to predict cross-flow VIV. A problem is that these models are not capable of accounting for non-linear structural response and time-varying flow.

While focus has been on avoidance of cross-flow VIV for decades, Sumer and Fredsøe (1997) pointed out the relevance of in-line VIV and a combination of the two phenomena. The vortex shedding frequency of in-line VIV is approximately twice as high compared to cross-flow VIV. Thus, in-line VIV generally occurs at lower flow velocities, also suggesting that fatigue damage from in-line VIV accumulates faster than fatigue damage from cross-flow VIV (Sumer & Fredsøe, 1997). The DNVGL response model approach (DNVGL-RP-F105, 2019) is commonly used as a design guideline with respect to in-line VIV. In this approach modal stresses and eigenfrequencies are used to estimate stress ranges that arise from VIV. It was developed for free spanning pipelines, thus, special considerations apply for non-straight pipes. However, for non-straight geometries it can be difficult to distinguish between the damage contribution from in-line VIV and cross-flow VIV, as they no longer occur in each other's neutral plane.

Model test results for the VIV response of an M-shaped jumper model were carried out by ExxonMobil and published by Wang et al. (2013), which allows for comparing potential VIV prediction approaches. In this test series, uniform bottom currents were simulated to achieve reduced velocities that excite the vibration modes of interest. A time domain VIV prediction model for the in-line and cross-flow directions has been developed at NTNU and is presented in Thorsen et al. (2014) and Ulveseter et al. (2017). The model has been implemented in the SINTEF Ocean computer program SIMLA together with a new bend element, allowing structural non-linearity, 3D flow and bend softening effects to be addressed.

The two main objectives of this paper are to show how this new element type affects the results in modal analysis and to demonstrate that the time domain tool is applicable for pipeline spool and jumper applications with non-straight parts.

2 METHODOLOGY AND MODEL

2.1 *General*

SIMLA is a finite element method-based program for non-linear static and dynamic analysis, specialized for pipe and cable simulations. Step-by-step time integration is used to describe load histories and analysis sequences (Sævik, 2017).

The pipe elements in SIMLA are formulated as standard two-node beam elements with 12 (2*6) degrees-of-freedom (DOF). The orientation and motion refer to a global coordinate system. For torsion rotation and axial displacement linear interpolation is applied, while cubic interpolation is used for transverse directions.

In SIMLA two models were made, of which one consisted of Pipe31 elements, referred to as Pipe31 model. The other one was modeled with Pipe34 elements in the bends adjacent to Pipe31 elements for the straight parts. This one is referred to as Pipe34 model. Pipe31 is an elastic pipe element, for which plane stress is assumed. All DOF are uncoupled from hoop stresses and hoop strains, since they are known from shell theory.

Pipe34 is a bend element type implemented with reference to Bathe et al. (1983). It is able to account for deformation of the cross-section and kinematic non-linearity. The ovalization of an initially circular cross-section due to bending during manufacturing is included in additional strain terms. Six ovalization DOF are introduced in addition to the twelve regular DOF. In contrast to the elbow elements from Bathe et al. (1983), Pipe34 is only linear-elastic.

To verify the use of Pipe34 elements as elbow elements, modal analysis was also performed in ABAQUS CAE version 6.13 on two models, of which one consisted of Pipe31 elements and the other one of Elbow31B elements in the bends and Pipe31 elements in the straight parts.

2.2 *Model*

The numerical model was built with reference to the model from the experiment published by Wang et al. (2013). It was built in model scale size with aluminium properties. The weight of the internal fluid was accounted for in the total unit mass. Both the structural weight and the weight of content were considered constant along the pipe. No internal pressure or free-surface effects inside the pipe were considered. With a scale ratio of 4.525 the model had a total arch length of 13.96 m. The lengths of each segment and the model properties are listed in Table 1 and Table 2, respectively. As in the experiment the model was placed one meter below sea surface. Figure 1 shows the jumper model in SIMLA with the locations where VIV was measured in the model test and where fatigue was evaluated in the simulation.

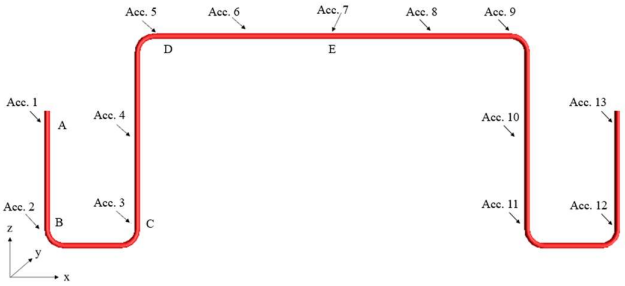

Figure 1: Jumper model in SIMLA with locations where VIV was measured in model tests (Acc.1-13) and where fatigue damage was calculated (A-E).

Table 1: Segment lengths of the model (Liu et al., 2020).

Segment name	Length [m]
Vertical 1	1.495
Horizontal 1	1.000
Vertical 2	2.323
Horizontal 2	4.327
Vertical 3	2.326
Horizontal 3	1.000
Vertical 4	1.495

Table 2: Jumper model properties (Wang et al., 2013).

Parameter	Value	Unit
Material density	2700	kg/m^3
Outer diameter	0.0605	m
Inner diameter	0.055	m
Wall thickness	2.77×10^{-3}	m
Elastic modulus (E)	6.90×10^{10}	N/m^2
Bending stiffness (EI)	1.44×10^{4}	Nm^2
Shear modulus (G)	2.61×10^{10}	N/m^2
Torsion stiffness (GJ)	1.08×10^{4}	Nm^2

The bends were modelled with a bending radius of three times the outer diameter of the pipe, which resulted in a bending radius of 0.1815 m. The number of elements was chosen in such way that the element length in bent pipe parts did not exceed the outer diameter size. Five elements per bend were used in the simulation, which led to an element length of 0.057 m. For the straight parts the element length was varied between once and twice the outer diameter. During modal analysis in SIMLA it was found that results converged with two diameter element length for the straight parts and one diameter element length for the bend parts.

2.3 *Modal analysis and stresses*

The required number of eigenvalues, starting with the smallest one, was found from a Lanczos solver both in SIMLA (Sævik et al., 2019) and in ABAQUS (SIMULIA, Dassault Systèmes, 2013), which was used for comparison. The number of relevant modes for this study was based on the maximum oscillation frequency that occurred during VIV simulations. In ABAQUS, the maximum principal stress was obtained directly. In SIMLA, information about axial

strain, torsion and the curvature in both transverse directions could be extracted from the output file from eigenvalue analysis for each mode shape. Data was given for each element in its local coordinate system and scaled with respect to the maximum modal displacement equal to one. To obtain unit stresses, the information had to be multiplied with the outer diameter. According to the DNVGL guidelines, total flexural stress was calculated at 16 points around the circumference in a local coordinate system:

$$\sigma_{xx} = -\kappa_y ER\cos\,\theta_i + \kappa_z ER\sin\,\theta_i \tag{1}$$

where the curvature κ was scaled with the outer diameter, E is the Young's modulus and R is the outer radius. The angle θ_i was specified for 16 points around the circumference. The maximum principal stress was then found with the equation:

$$\sigma_1 = \frac{\sigma_{xx}}{2} + \sqrt{\left(\frac{\sigma_{xx}}{2}\right)^2 + \tau_{xy}^2} \tag{2}$$

The shear stress about the longitudinal pipe axis was calculated as:

$$\tau_{xy} = \varphi_{,x} GR \tag{3}$$

where the torsion $\varphi_{,x}$ was given in radians per meter and scaled with the outer diameter, and G is the shear modulus.

2.4 *VIV prediction model*

The principles of the model are described in Thorsen (2016), Thorsen et al. (2014) and Ulveseter et al. (2017). The most important feature is the ability to synchronize fluid forces with cylinder motion. Synchronization provides the possibility to transfer energy to the cylinder at specific frequencies and motion amplitudes (Ulveseter et al., 2017). This also allows the vortex-shedding frequency to lock on to the structure's frequency of oscillation.

Both cross-flow and in-line VIV can be analyzed in SIMLA. The program applies additional vortex-shedding terms to the Morison equation together with the synchronization model. The decision to switch between cross-flow or in-line forces is made based on comparison of the amplitudes. A synchronization model for cross-flow-induced in-line VIV is also included. To compare results from the VIV prediction tool with experimental data, non-dimensional response amplitudes were plotted against reduced velocities.

To find the active mode for each load case, Fast Fourier Transformation (FTT) was applied to transfer the signal into frequency domain. From the location of the peak value, the oscillating frequency was found. The active mode was then identified as the one with its natural frequency closest to the structure's oscillating frequency.

2.5 *Fatigue analysis*

Fatigue damage was obtained from two methods, of which the first one utilized the moment output from SIMLA and applied rainflow counting on stress cycles. The second method was the DNVGL response model procedure (DNVGL-RP-F105, 2019), for which the modal analysis results were applied together with empirical equations.

For fatigue analysis in SIMLA, mode identification during VIV was not necessary, since forces and moments in all DOF were obtained as time signals. As for modal stresses, the flexural stresses were evaluated at 16 points around the jumper circumference; see Eq. (4). Flexural stresses were found from the moments around the y- and z-axis in a local coordinate system. The x-axis is aligned with the pipe axis as shown in Figure 2.

$$\sigma_{xx} = -\frac{M_y}{I_y} R\sin\,\theta_i + \frac{M_z}{I_z} R\cos\,\theta_i \tag{4}$$

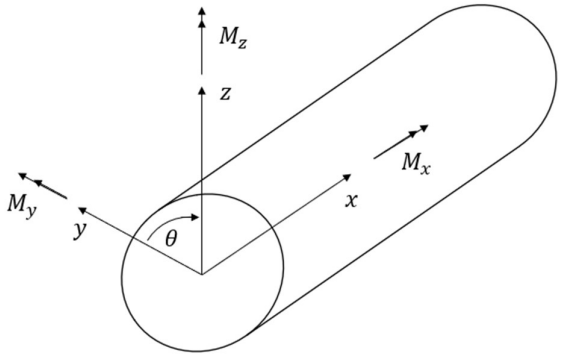

Figure 2: Pipe element with its local coordinate system.

The area moments of inertia, I_y and I_z, were calculated with the equation for thin-walled circular cross-sections as:

$$I_y = I_z = \pi R^3 t \tag{5}$$

The shear stress was constant around the circumference of each pipe section and calculated as:

$$\tau_{xy} = \frac{M_x}{I_x} R \tag{6}$$

where the polar moment of inertia I_x equals $2\pi R^3 t$. From the two stress signals, the maximum principal stress was calculated with Eq. (2) at each time step. To the best of knowledge, the first principal stress criterion gives conservative results, since the maximum stress is assumed to contribute to crack-opening regardless of the real stress direction. When calculated

at each time step, shifts between flexural and torsional stress cycles should also be taken care of. To transform the signal of oscillating stresses into a set of stress reversals with constant amplitudes a rainflow counting algorithm was used. The equivalent stress range was found by the direct summation method (Berge & Ås, 2017):

$$\Delta S_{eq} = \left[\frac{\Sigma_i n_i (\Delta S_i)^m}{\Sigma_i n_i}\right]^{\frac{1}{m}} \quad (7)$$

where n_i is the number of cycles for one set in the histogram, ΔS_i is the stress range of the corresponding set and m is a constant of applied SN-curve. Fatigue was calculated and compared for each load case under the assumption that it is present over one year with a probability of occurrence of 100 percent.

For the second method, the DNVGL response model procedure was followed. Based on empirical Table 3 and Table 4, so that in-plane bending occurs at a lower frequency than out-of-plane twist for the elbow models. This is in correlation with the observations from the test.

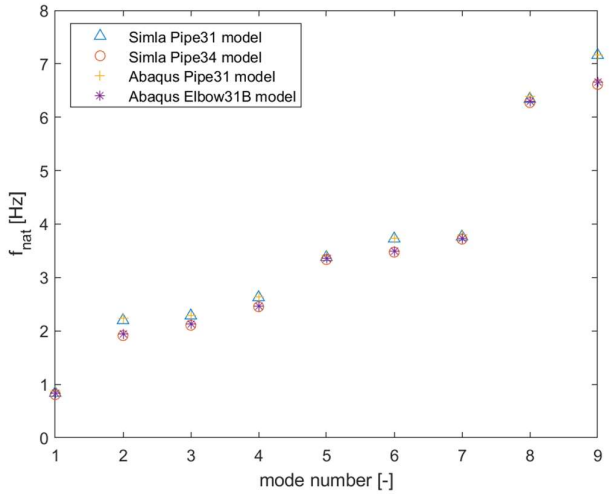

Figure 3: Comparison of natural frequencies in SIMLA and ABAQUS.

Mode shapes of the two elbow element models are identical. Both Pipe34 and Elbow31B elements are beam elements for which Von Karman correction is applied to model the deformation of the cross-section. The derogation of results between SIMLA models and ABAQUS models can be attributed to the differences of Pipe31 elements. Pipe31 elements in ABAQUS are Timoshenko beams which allow for transverse shear deformation. In SIMLA, on the contrary, the cross-section of Pipe31 elements remains plane and does not distort due to transverse shear. It should be pointed out that the shift in mode shapes could not be obtained with models consisting only of Pipe31 elements, even with a refined mesh. This gives a relevant reason to use elbow elements in the analysis of subsea jumpers.

response amplitudes and the modal stresses obtained from FEA, combined stress ranges for cross-flow VIV and in-line VIV including cross-flow-induced in-line VIV could be calculated by following the procedure described in the recommended practice DNVGL-RP-F105 (2019). For non-straight pipes, no mode competition is applied, which means that all modes that could be active based on their reduced velocity apply their full stress range.

3 EFFECT OF ELBOW ELEMENTS

3.1 *Eigenfrequencies and mode shapes*

Eigenfrequencies for the Pipe34 model in SIMLA and the Elbow31B model in ABAQUS are generally lower than the ones from the Pipe31 models, as shown in Figure 3. Moreover, mode two and three are switched in order as shown in

3.2 *Modal stresses*

An overview of modal stresses for the first nine modes is given in Figure 4 and Figure 5, where the maximum principal stress is shown for the Pipe31 and Pipe34 models in SIMLA. For the Pipe34 model, the resulting stress in the bends was increased up to factor

Table 3: Eigenfrequencies and mode shapes of Pipe31 models.

Mode	f_n in SIMLA [Hz]	f_n in ABAQUS [Hz]	Mode shape
1	0.8377	0.8744	out-of-plane bending in *y*-direction with largest displacement at top horizontal
2	2.1991	2.2343	out-of-plane twist around center point of top horizontal
3	2.2859	2.2844	in-plane bending in *x*-direction
4	2.6285	2.6341	in-plane bending in *z*-direction

Table 4: Eigenfrequencies and mode shapes of Pipe34 model (SIMLA) and Elbow31B model (ABAQUS).

Mode	f_n in SIMLA [Hz]	f_n in ABAQUS [Hz]	Mode shape
1	0.8076	0.8336	out-of-plane bending in *y*-direction with largest displacement at top horizontal
2	1.9131	1.9406	in-plane bending in *x*-direction
3	2.1047	2.1344	out-of-plane twist around center point of top horizontal

two compared with the Pipe31 model. In the adjacent straight parts, on the other hand, the stresses were decreased by up to 35 percent. The coupled effect of decreased stresses in straight parts and increased stresses in bends was most significant for the in-plane bending modes, which were modes two, four, six and nine for the model including Pipe34 elements. Generally, largest principal stresses occurred at the boundaries or in the midpoint of the top horizontal for the Pipe31 model, while they occurred in bends for the Pipe34 model. The difference was due to the flexural stress component. Torsional stresses had the same magnitude for both models.

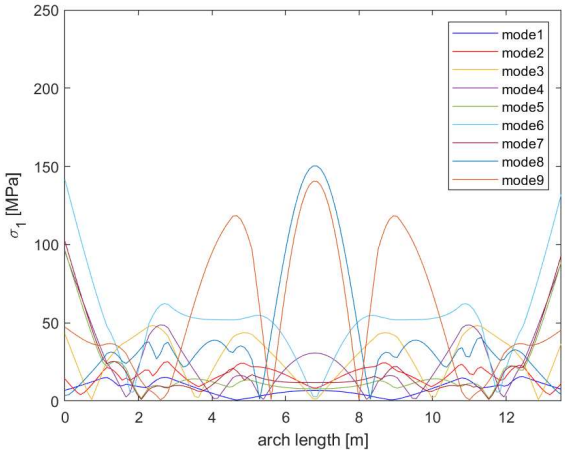

Figure 4: Maximum principal unit stress of the first nine modes for the SIMLA Pipe31 model. Scaled with the outer diameter and the maximum modal displacement.

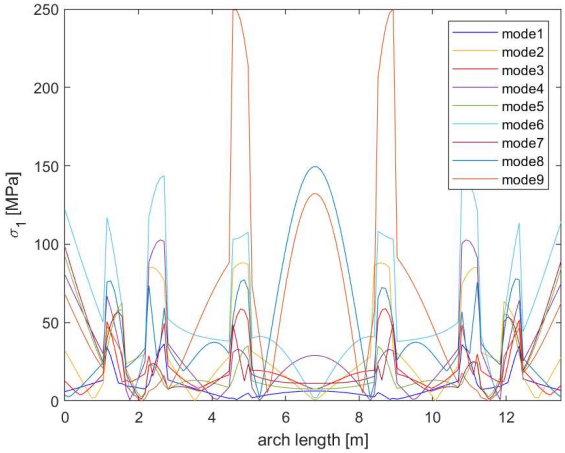

Figure 5: Maximum principal unit stress of the first nine modes for the SIMLA Pipe34 model. Scaled with the outer diameter and the maximum modal displacement.

4 PARAMETER STUDY OF THE TIME DOMAIN MODEL

Some parameters of the time domain model were modified to apply it on non-straight geometries. A challenge was that the response of a jumper was entirely different when the angle of attack changed. The parameters were chosen so that conservative results were obtained for the three observed flow directions of ten, 45 and 90 degrees. The cross-flow lift force coefficient and the in-line force coefficient for instability region one were increased, since for both the 10- and 90-degree angle out-of-plane bending occurred in the model test with large amplitudes. From their default values of 1.0 and 0.8, respectively, the coefficients were both set to 1.2.

The minimum non-dimensional vibration frequency that gives energy input for in-line region one, $\hat{f}_{1I1}$ in SIMLA, had to be modified in such way that in-line VIV could be activated in a wider range of reduced velocities. Since it is a non-dimensional quantity, the reduced velocity range where in-line VIV can be activated is approximately the inverse of $\hat{f}_{1I1}$. It is not exactly equal to this value, because reduced velocity was calculated with the natural frequency that was found closest to the vibration frequency and not with the vibration frequency itself. For the jumper model, in-line VIV is not limited to the low velocity range. From experimental data, it was observed that large displacement in in-line direction could occur for reduced velocities of up to eight. This is in agreement with the paper by Wang et al. (2018) who investigated the coupling of in-line and cross-flow motion and reported that in-line motion contributed to the path described by cylinder motion for the non-dimensional reduced velocity of eight, while at a value of ten, the in-line motion was negligible. Therefore, $\hat{f}_{1I1}$ was set to 0.13. With this value conservative results were obtained for all three flow directions.

5 VIV SIMULATION RESULTS AND COMPARISON

5.1 *VIV motion*

Experimental data was available for accelerometer positions three and five for the 10-degree flow and accelerometers three and seven for the 45- and 90-degree flow. Accelerometer five was located on the top horizontal part, H2, next to the bend, while number seven was located at the center of H2. Accelerometer three was placed at the lower part of the jumper, next to the bend at vertical part V2, as shown in Figure 1. The model setup in towing tank is shown in Figure 6 from Wang et al. (2013).

For the 10-degree flow, the VIV amplitudes were very stable when a steady current velocity was applied. In Figure 7 and Figure 8 simulation results for this flow angle are plotted together with experimental data from Wang et al. (2013) and the DNVGL response model curves. The cross-flow response model

depends on modal frequencies, thus, it is plotted for both the Pipe31 and Pipe34 model. For better comparability the response models were calculated without additional safety as all safety factors were set to 1.0.

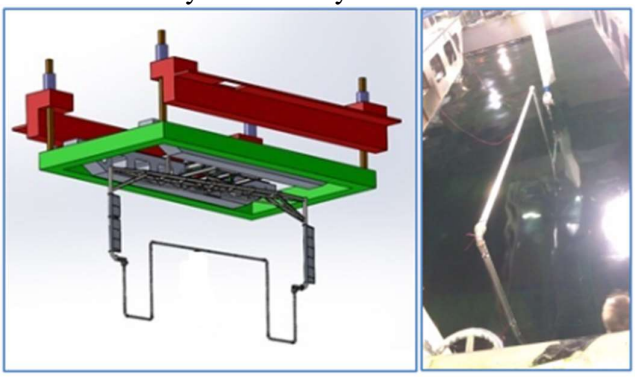

Figure 6: Model setup in towing tank (Wang et al., 2013)

From the oscillating frequencies it was concluded that the in-plane bending mode (mode three for Pipe31 and mode two for Pipe34 model) was active for low current velocities up to 0.2 m/s. From 0.25 m/s the out-of-plane bending mode (mode one) was active. Transition to the twist mode (mode two for Pipe31 and mode three for Pipe34 model) occurred between 0.50 and 0.55 m/s for the Pipe34 model and between 0.6 and 0.65 m/s for the Pipe31 model. The earlier transition of the Pipe34 model is in better agreement with observations from the model test reported by Wang et al. (2013). In *x*-direction significant response from the simulations and test data was observed around a non-dimensional reduced velocity of 1.7, which is linked to the first in-line instability region and first lock-in region. The largest amplitudes here occurred in the simulations with current velocities of 0.15 and 0.2 m/s. About twice as large in-line response compared to the first instability region occurred at reduced velocities between six and eight, presumably due to cross-flow-induced in-line VIV. Peak values for pure cross-flow VIV in the *y*-direction were observed at reduced velocities of six to eight, which is in agreement with the model test. As mentioned previously, model test results showed quite narrow peaks, while they were spread wider in SIMLA results. However, the time domain model results were in a conservative range.

For the 90-degree flow, unsteady amplitudes were observed when the current velocity changed and for the highest load cases, especially in the *y*-direction. From the model test it was reported that the end dynamometers had reached their load capacity and, thus, tests were not continued beyond 0.79 m/s; see Wang et al. (2013). For this flow angle the response in the *y*-direction, which is associated with in-line VIV, dominated for both models up to 0.3 m/s. The oscillating frequency was closest to the first modal frequency. For further increased current velocities, from 0.4 to 0.65 m/s the in-plane bending mode (mode three and two for Pipe31 and Pipe34 model, respectively) was active with largest non-dimensional amplitudes in the *x*-direction. For the 90-degree flow, this is associated with cross-flow VIV. Due to decreased stiffness, the Pipe34 model shows significantly larger responses in the *x*-direction for the above-mentioned flow velocities. This is presented in Figure 9 for reduced velocities around five. Nonetheless, the peak values which occur at reduced velocities around six are in agreement for both models and in good correlation with experimental results.

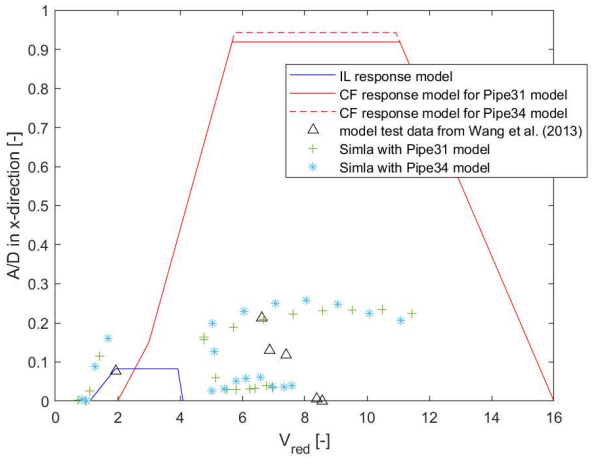

Figure 7: Comparison of VIV response in the *x*-direction for the 10-degree flow at accelerometer five.

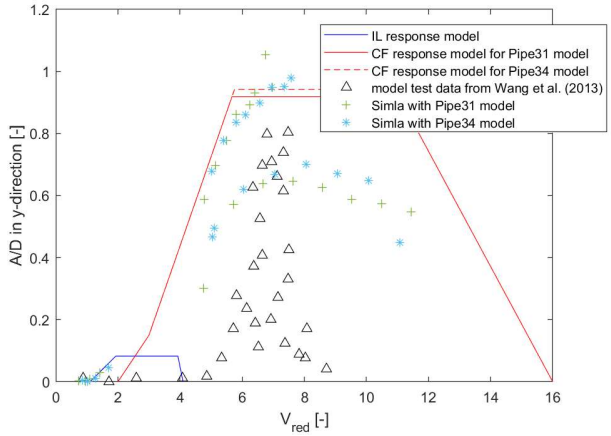

Figure 8: Comparison of VIV response in the *y*-direction for the 10-degree flow at accelerometer five.

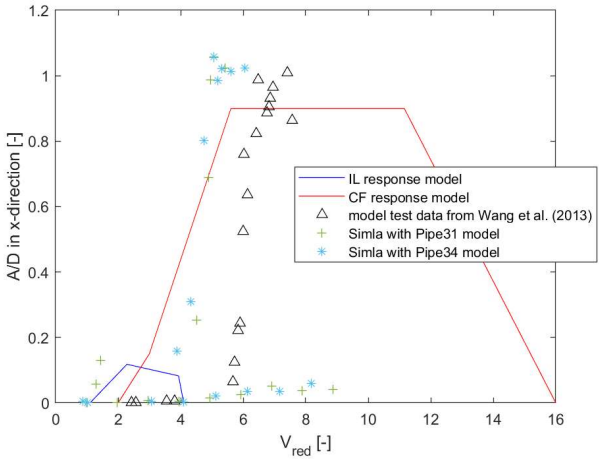

Figure 9: Comparison of VIV response in the *x*-direction for the 90-degree flow at accelerometer seven.

5.2 *Fatigue damage*

Stress ranges for fatigue calculations were assessed by the two methods at locations A-E. Since welds are usually placed next to the bend parts, but with a small offset, the elements next to the bends and at the longer of two adjacent straight parts were chosen as locations B to D.

For the 10-degree flow, torsional moments were very small in the in-line VIV region up to 0.2 m/s. For higher current velocities, the contribution from torsional stresses increased and became significant for current velocities of 0.6 m/s and higher at locations C, D and E. This is presented in Figure 10 for location E. Closer to the supports, at locations A and B, torsional stresses remained comparatively small for this flow angle and fatigue estimates from the first principal stress were dominated by flexural stresses. For both methods the overall fatigue damage had its maximum at location A. For current velocities 0.05 and 0.1 m/s SIMLA gave larger fatigue estimates, while for the higher current velocities, the response model procedure predicted significantly higher fatigue damage, as shown in Figure 11.

For the 90-degree flow, several load cases showed larger torsion moments than flexural moments. Further, the flexural moments were more unsteady in the same regions. Close to the bends, this was observed for current velocities of 0.3 to 0.5 m/s, as shown in Figure 12 for location B. However, the largest fatigue damage occurred at the supports, presented in Figure 13. For current velocities up to 0.3 m/s, the SIMLA model gave larger fatigue damage, while for all higher load cases the DNVGL response model gave higher fatigue estimates. The largest difference occurred at 0.5 m/s, because in the response model procedure, the flexural stress contribution to fatigue damage was increased steadily, but in SIMLA strong flexural stress response only arose beyond that.

For the 45-degree flow, similar observations were made as for the 90-degree flow with dominating torsion moments for 0.4 to 0.6 m/s at location B. Only at this flow angle gave the time domain model higher fatigue estimates for the current velocities 0.7 to 0.9 m/s compared to the response model. However, too few data were available to draw conclusions on whether the parameters of the time domain model could be adjusted for flow angles between 10 and 90 degrees.

From the VIV motion amplitudes, it was already shown that the DNVGL procedure gives higher response estimates for many reduced velocities compared to the SIMLA results and model test data. In SIMLA, several modes can be active at the same time, too, but not all apply their full stress range. At the shorter segments, where higher modes were identified during VIV, the response amplitudes in SIMLA were significantly lower than from the guidelines. Following the DNVGL procedure, higher modes contributed with their full stresses without mode competition. It is notable that for some cases with low velocity currents SIMLA gave larger fatigue estimates, however, fatigue damage for these cases was small in general.

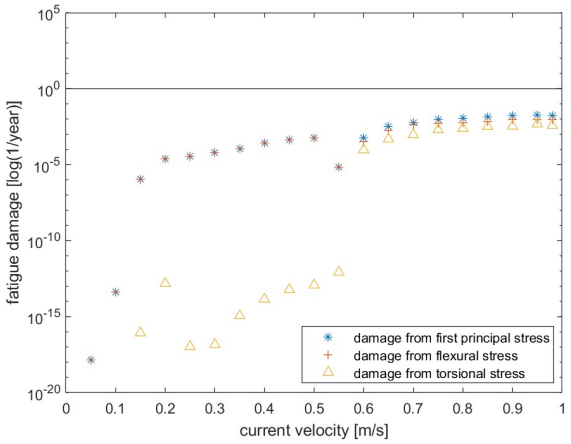

Figure 10: Fatigue damage for the Pipe34 model in SIMLA in 10-degree flow at location E.

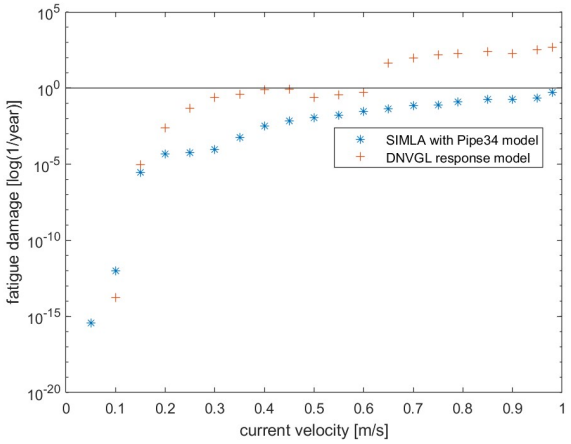

Figure 11: Comparison of fatigue damage from first principal stresses for the Pipe34 model in SIMLA and with the response model procedure in 10-degree flow at location A.

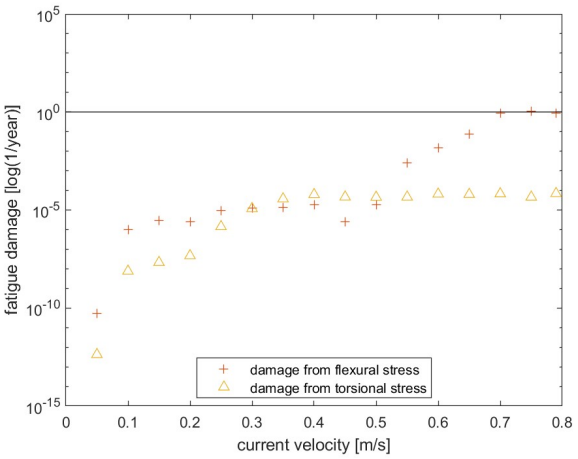

Figure 12: Comparison of fatigue damage from flexural and torsional stresses for the Pipe34 model in SIMLA in 90-degree flow at location B.

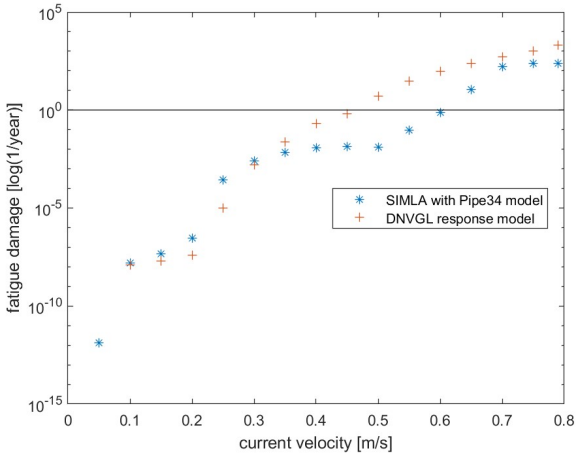

Figure 13: Comparison of fatigue damage from first principal stresses for the Pipe34 model in SIMLA and with the response model procedure in 90-degree flow at location A.

6 CONCLUSIONS

This study presented the application of a time domain model for VIV on a model-scale jumper with regular pipe elements (Pipe31) and elbow elements (Pipe34) in the bends. It was shown that the modal results of models using elbow elements were in better agreement with results from the model test, since the first in-plane bending mode had a lower natural frequency compared to the out-of-plane twist mode due to the softer bends. The dominating VIV response with respect to direction of motion and location along the jumper could be associated with one of the first four modes for all three flow directions. Thus, these four modes require highest standards of accuracy. In the direction where smaller VIV motion occurred and at the shorter jumper segments, also higher modal frequencies were identified.

Regarding VIV motion, the SIMLA results were in a conservative range and in good correlation with test data. Thus, the VIV model is promising for non-straight geometries. The shift from one oscillation pattern to another one (with respect to oscillating frequency and direction of largest amplitudes) for consecutive load cases happened at lower current velocities for the Pipe34 model than for the Pipe31 model. The largest fatigue damage was observed at the jumper supports for all three flow directions. The largest deviations of fatigue estimates from the two methods also occurred at this location. Except for the lowest current velocities and several cases in the 45-degree flow, fatigue damage from the DNV GL response models was significantly higher than obtained from SIMLA. This was because the response model procedure assumes that all active modes contribute with their full stress range for non-straight pipes. In the time domain model, several modes were active in the same load case, too, but they have the possibility to compete with each other and contribute with less than the full amount. The smallest difference between the two methods was observed at the center of the top

horizontal. Torsional stresses were relevant for all three flow directions. Especially for the 45- and 90-degree flow and at the lower jumper segment, the contribution to fatigue damage was significant.

7 REFERENCES

Bathe, K-J., Almeida, C. A. & Ho, L. W. 1983. A simple and effective pipe elbow element – some nonlinear capabilities. *Computers & Structures,* 17(5-6): 659-667. https://doi.org/10.1016/0045-7949(83)90079-2

Berge, S. & Ås, S.K. 2017. Compendium: Fatigue and Fracture Design of Marine Structures. NTNU.

DNVGL-RP-F105. 2019. Recommended practice. Free spanning pipelines. DNV-GL.

Larsen, C.M., Lie, H., Passano, E., Yttervik, R., Wu, J., Baarholm, G.S. 2017. VIVANA-Theory Manual, 4.10.1. SINTEF Ocean. Trondheim, Norway.

Liu, Z., Igeh, L. A., Wu, J. and Ong, M. C. 2020. Fatigue damage assessment to a rigid planar jumper on model scale. ASME. *Journal of Offshore Mechanics and Arctic Engineering,* February 2020; 142(1): 011602. https://doi.org/10.1115/1.4044074

Sævik, S. 2017. SIMLA-Theory manual. SINTEF Ocean. Trondheim, Norway.

Sævik, S., Baarholm, G. S., Økland, O. D. & Gjøsteen, J. K. 2019. SIMLA Version 3.16.0 User manual. SINTEF Ocean.

SIMULIA, Dassault Systèmes. 2013. Abaqus Analysis User's Guide, v. 6.13. Johnston, RI.

Sumer, B. M. & Fredsøe, J. 1997. Forces on a cylinder in regular waves. *Hydrodynamics around cylindrical structures, Advanced series on ocean engineering,* 12: 123-209. World Scientific. https://doi.org/10.1142/6248.

Thorsen, M. J., Sævik, S. & Larsen, C.M. 2014. A simplified method for time domain simulation of cross-flow vortex-induced vibrations. *Journal of Fluids and Structures,* 49: 135-148. https://doi.org/10.1016/j.jfluidstructs.2014.04.006.

Thorsen, M. J. 2016. Time domain analysis of vortex-induced vibrations. Doctoral thesis at NTNU;2016:231. http://hdl.handle.net/11250/2414408.

Triantafyllou, M., Triantafyllou, G., Tein, Y.S.D., Ambrose, B.D. 1999. Pragmatic riser VIV analysis. Proc. Offshore Technology Conference, Houston. OTC. 3. 10.4043/10931-MS.

Ulveseter, J. V., Sævik, S. & Larsen, C.M. 2017. Time domain model for calculation of pure in-line vortex-induced vibrations. *Journal of Fluids and Structures,* 68:158–173. https://doi.org/10.1016/j.jfluidstructs.2016.10.013.

Vandiver, J.K., Li, L. 2005. SHEAR7 V4.4 Program Theoretical Manual. Department of Ocean Engineering, Massachusetts Institute of Technology. Cambridge, MA.

Wang, H., Huang, J., Lee, S., Gioielli, P., Kan, W., Spencer, D. & Islam, M. 2013. VIV response of a subsea jumper in uniform current. In *Proceedings of the ASME 2013 32nd International Conference on Ocean, Offshore and Arctic Engineering. Volume 4B: Pipeline and Riser Technology.* Nantes, France. June 9–14, 2013. V04BT04A043. ASME. https://doi.org/10.1115/OMAE2013-11417.

Wang, K., Ji, C., Chi, Q., & Wu, H. 2018. Hydrodynamic force investigation of a rigid cylinder under the coupling CF and IL motion. *Journal of Fluids and Structures,* 81: 598-616. https://doi.org/10.1016/j.jfluidstructs.2018.06.004